JACS
JOURNAL OF THE AMERICAN CHEMICAL SOCIETY
pubs.acs.org/JACS
Article

Modulating Singlet Fission by Scanning through Vibronic Resonances in Pentacene-Based Blends

Frederik Unger, Luca Moretti,[⊥] Julian Hausch,[⊥] Jona Bredehoeft, Clemens Zeiser, Sara Haug, Roel Tempelaar, Nicholas J. Hestand,* Giulio Cerullo,* and Katharina Broch*

Cite This: J. Am. Chem. Soc. 2022, 144, 20610−20619
Read Online

ACCESS | Metrics & More | Article Recommendations | Supporting Information

ABSTRACT: Vibronic coupling has been proposed to play a decisive role in promoting ultrafast singlet fission (SF), the conversion of a singlet exciton into two triplet excitons. Its inherent complexity is challenging to explore, both from a theoretical and an experimental point of view, due to the variety of potentially relevant vibrational modes. Here, we report a study on blends of the prototypical SF chromophore pentacene in which we engineer the polarizability of the molecular environment to scan the energy of the excited singlet state (S_1) continuously over a narrow energy range, covering vibrational sublevels of the triplet-pair state (^{1}(TT)). Using femtosecond transient absorption spectroscopy, we probe the dependence of the SF rate on energetic resonance between vibronic states and, by comparison with simulation, identify vibrational modes near 1150 cm^{-1} as key in facilitating ultrafast SF in pentacene.

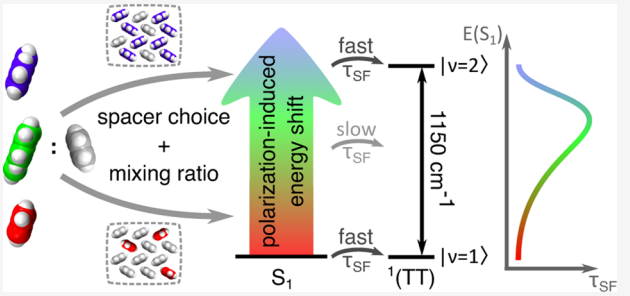

INTRODUCTION

Due to its potential to increase the solar cell power conversion efficiency above the Shockley−Queisser limit,[1] singlet fission (SF) has gained interest throughout the past decade.[2] SF describes the photophysical process in which a singlet exciton (S_1) splits up into two triplet excitons ($2 \times T_1$) via ^{1}(TT), a multiexcitonic state of singlet character.[2−5] There is an ongoing debate about what controls the first step of SF, namely, the conversion from S_1 to ^{1}(TT). Multiple experimental[6−13] and theoretical[14−17] studies have emphasized the role of relative molecular orientation[6,10−13,16] and contributions from real or virtual charge-transfer states.[7−9,14,15,17−21] In addition, motivated by theoretical modeling,[15,22−24] the importance of vibrations in mediating the electronic coupling between S_1 and ^{1}(TT)[13,22,25−29] has been investigated. While pioneering studies employed sophisticated experimental techniques[13,22,26−28] to probe vibronic coherences, precisely controlling the energetic resonance between the involved states was not a focus. A first approach to address the latter used chemical modification,[4,22,30,31] but this strategy alters electronic properties, crystal geometry, intermolecular interactions, and vibronic coupling at the same time,[22] making it challenging to disentangle their contributions to SF. Furthermore, this approach only allows for discrete changes in the energy difference between S_1 and ^{1}(TT) and limits the study to a subset of available vibrational modes in the relevant energy range, that is, a few hundred meV. Computational simulations face a similar challenge due to unfavorably increasing computational costs with increasing number of considered vibrational modes.[24] Therefore, neither simulation nor experiment can easily address the full diversity of vibrational modes and their role in the SF process, in particular due to lacking experimental feasibility in continuously scanning through energetic resonances.

Here, we demonstrate that statistically intermixed blends of a SF molecule with a weakly interacting spacer molecule can be an elegant way to tackle this challenge and to probe the role of vibronic coupling in SF, providing a benchmark against which current theories can be tested. There are two main benefits of using such blends: first, structural properties, and in particular the packing motif, are preserved compared to neat films, allowing for unambiguous conclusions, and second, the energy of electronic states may be indirectly tuned through changes in the polarizability of the molecular environment.[32,33] With the latter, energetic shifts up to hundreds of meV can be induced in the electronic states of significant charge-transfer character such as S_1.[14,34] Since the localized nature of both S_0 and ^{1}(TT)[23,35−38] makes their energy rather insensitive to changes in the polarizability of the molecular environment,[39] we can thus controllably scan S_1 over ^{1}(TT) and its vibrational sublevels.

This polarizability-induced tuning of excited-state energetics is here exploited by combining pentacene (PEN), a prototypical

Received: July 10, 2022
Published: November 1, 2022

Downloaded via POLITECNICO DI MILANO on January 10, 2023 at 10:03:57 (UTC).
See https://pubs.acs.org/sharingguidelines for options on how to legitimately share published articles.

SF chromophore,[2,40] with three spacer molecules of increasing optical band gap and concomitantly decreasing polarizability,[41] namely, anthradithiophene (ADT), dinaphthothienothiophene (DNTT), and [6]phenacene (6PH) (Figure 1a–c). By

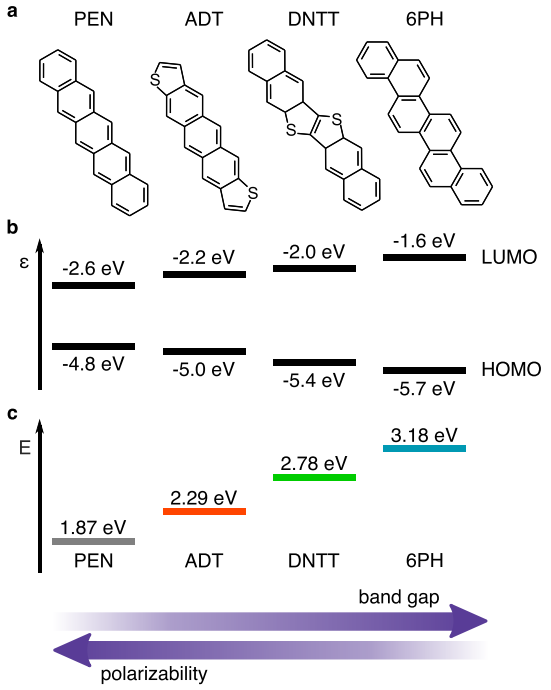

Figure 1. Chemical structures, orbital energies, and optical band gaps. (a) Chemical structures of PEN, ADT, DNTT, and 6PH (from left to right). (b) HOMO and LUMO energies determined by DFT (B3-LYP/def-TZVP). (c) Optical band gaps determined from UV/Vis transmission spectroscopy of neat films (see Figure S7 in the Supporting Information).

changing the spacer molecule and adjusting the mixing ratio, we are able to continuously scan the energy of S_1 relative to ^{1}(TT) and its vibrational sublevels, spanning an energetic range covering the relevant vibrational modes. The resulting changes in the SF time constant are probed by femtosecond transient absorption (TA) spectroscopy and complemented by simulations of the ^{1}(TT) population dynamics as a function of the energetic difference between the relevant states. Thus, we experimentally confirm the important role of vibrational modes near 1150 cm^{-1} (143 meV) that have been suggested as key for SF in PEN.[7,22,24] The strategy presented here enables us to continuously and controllably scan through energetic resonances between vibronic states, providing access to the microscopic details of ultrafast SF on a level which we believe is challenging to achieve by other approaches.

RESULTS AND DISCUSSION

Controlling the energetic difference between vibronic states using blends puts specific demands on the chemical, optical, and structural properties of the spacer molecules in relation to the SF chromophore, here PEN. These requirements were the basis for our choice of spacer molecules, see Figure 1a. In particular, the energetic position of their HOMO and LUMO relative to PEN must ensure weak interaction in the blends (Figure 1b), so that the main effect of the spacer molecules is to change the polarizability of the environment. The extent of this change can be controlled by the optical band gap (Figures 1c and S7 in the Supporting Information), which is linked to the polarizability. Based on the literature,[41] we expect the polarizability to decrease with increasing band gap (see arrows in Figure 1c) and, thus, the energy of S_1 in PEN ($E(S_1)$) to increase within the blends following the evolution of the band gap, that is, from ADT to DNTT to 6PH, vide infra, comparable to the solvatochromic effect. Finally, in order to obtain a continuous change in $E(S_1)$, statistical intermixing over a large range of concentrations is required, which is facilitated by the similarity in size between the molecules[42] (see Figures 1a and S2–S5 in the Supporting Information for X-ray diffraction results, which demonstrate the existence of long-range order in the mixed films as well as a linear trend in the lattice parameters with mixing ratio following Vegard's law for binary solid solutions[43]) and in accordance with previous reports in the literature on similar systems.[32,33,44,45] Therefore, the use of three spacer molecules differing in their polarizability in combination with the mixing behavior allows for a continuous variation in $E(S_1)$ over a wide range.

Figure 2a compares the steady-state absorption spectra of PEN blends with the three different spacer molecules for various PEN fractions, f_{PEN}. Focusing on the evolution of the absorption features below 2.1 eV, which are assigned to the Davydov splitting (DS) in PEN,[14,32] two clear trends for $E(S_1)$, determined from the position of the lower Davydov component, can be observed. *Within* a series, the shift to higher energies (hypsochromic) becomes more pronounced with decreasing f_{PEN}, while *between* the series, the hypsochromic shift of $E(S_1)$ increases with increasing band gap of the spacer molecule for a given PEN fraction. This is illustrated in Figure 2b for the blends with 20% PEN and supports the expected inverse correlation between the band gap of a molecule and its polarizability as detailed before. The two trends can be rationalized by the mixing-ratio- and spacer-molecule-dependent change in polarizability of the molecular environment of a given PEN molecule in the blends compared to in a neat PEN film. When a PEN molecule is replaced by a spacer molecule, the polarizability of the environment decreases, causing a destabilization of the S_1 state and a hypsochromic spectral shift of the $S_1 \leftarrow S_0$ transition.[41] The magnitude of the destabilization, and therefore of the hypsochromic shift, depends on the polarizability of the spacer molecule, as discussed before, leading to the difference between the series, but also on the average number of PEN neighbors, leading to a continuous increase in $E(S_1)$ within a series.[32,33] We note that the large energetic shift of the absorption spectra of the 20% blends compared to PEN in solution (dotted line in Figure 2b) indicates the existence of a long range order even at such low PEN concentrations and is in contrast to previous studies on amorphous films[46] (see the Supporting Information for details). The mixing-ratio- and spacer-molecule-dependent hypsochromic shift can be quantified by fitting the region of the DS (see Figure 2c), demonstrating our fine control of $E(S_1)$ in the blends.

Importantly, the relative energy of the triplet state T_1 in PEN, $E(T_1)$, compared to S_0, is robust with respect to changes in the molecular environment[22,39] due to its localized nature.[35–37] This assumption is supported by comparing the experimentally determined singlet- and triplet-state energies in the gas phase and in the condensed state,[47–50] which show a significantly higher dependence of the former on the polarizability of the environment compared to the latter. In conjunction with the expected weak interaction of the triplets and the small charge-transfer contribution (vide infra),[19,51–53] this allows us to

https://doi.org/10.1021/jacs.2c07237
J. Am. Chem. Soc. 2022, 144, 20610–20619

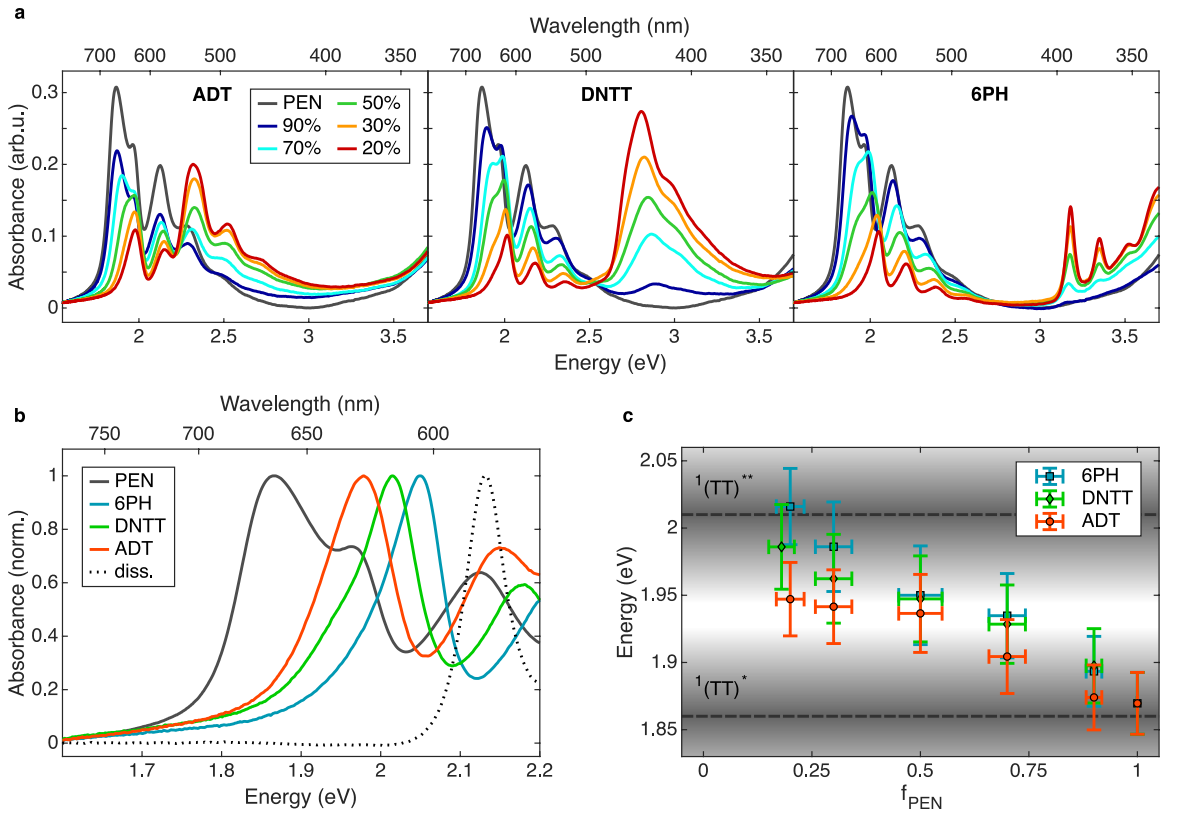

Figure 2. Steady-state optical properties. (a) UV/vis absorption spectra for blends of PEN with ADT, DNTT, and 6PH. (b) UV/vis absorption spectra for blends of 20% PEN alongside neat PEN in a thin film and in dichlorobenzene solution (monomer, dotted line) for comparison. The shift to higher energies (hypsochromic shift) is most pronounced for the blend with 6PH and smallest for the blend with ADT in accordance with the band gap of the spacer molecule. (c) Evolution of $E(S_1)$ in the three series relative to the energy of ^{1}(TT) dressed by one or two vibrational quanta of frequency 1150 cm^{-1} (143 meV), denoted as ^{1}(TT)* and ^{1}(TT)**, respectively, see the dashed horizontal lines. Horizontal error bars correspond to the error of the quartz crystal microbalances used for thickness determination and vertical error bars are proportional to the full width at half-maximum (FWHM) of Gaussian functions fitted to absorption peaks. The possible energy distribution of ^{1}(TT) due to inhomogeneous broadening is illustrated by the gray color gradient, assuming a Gaussian standard deviation of σ = 27 meV.[23]

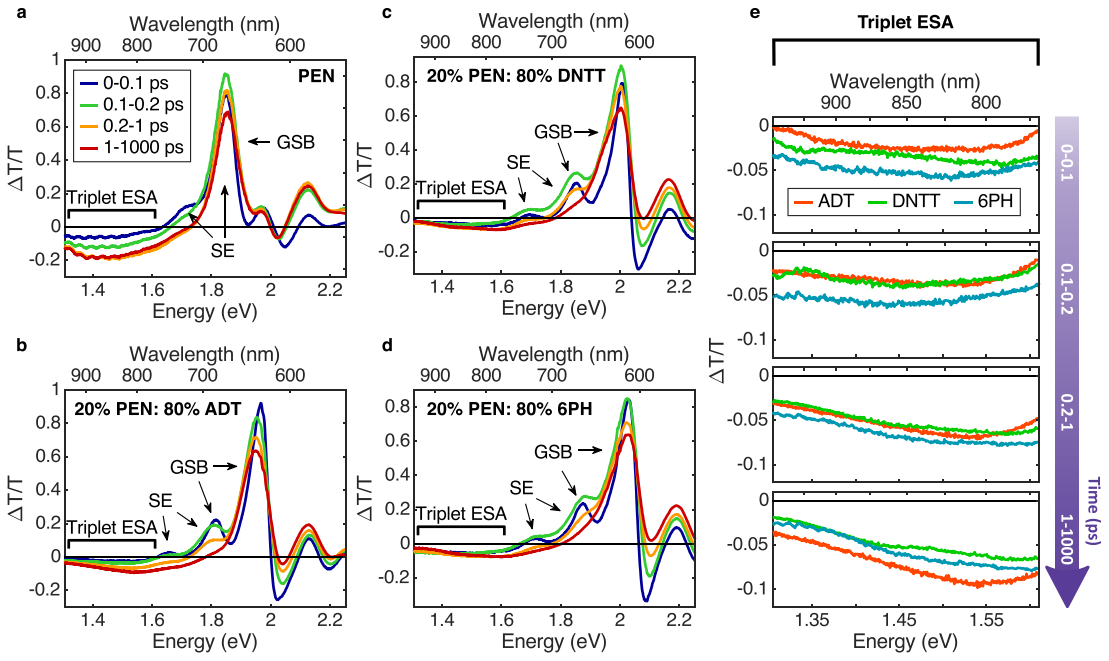

Figure 3. TA spectra at different delay times. (a–d) TA spectra for neat PEN and 20% PEN blends with spacer molecules ADT, DNTT, and 6PH averaged over the indicated delay times. The GSB is indicated along with features from SE and triplet ESA. (e) Zoom into the region of the triplet ESA for different delay times for the 20% PEN blends, see Figure 4 for the corresponding time traces.

https://doi.org/10.1021/jacs.2c07237
J. Am. Chem. Soc. 2022, 144, 20610−20619

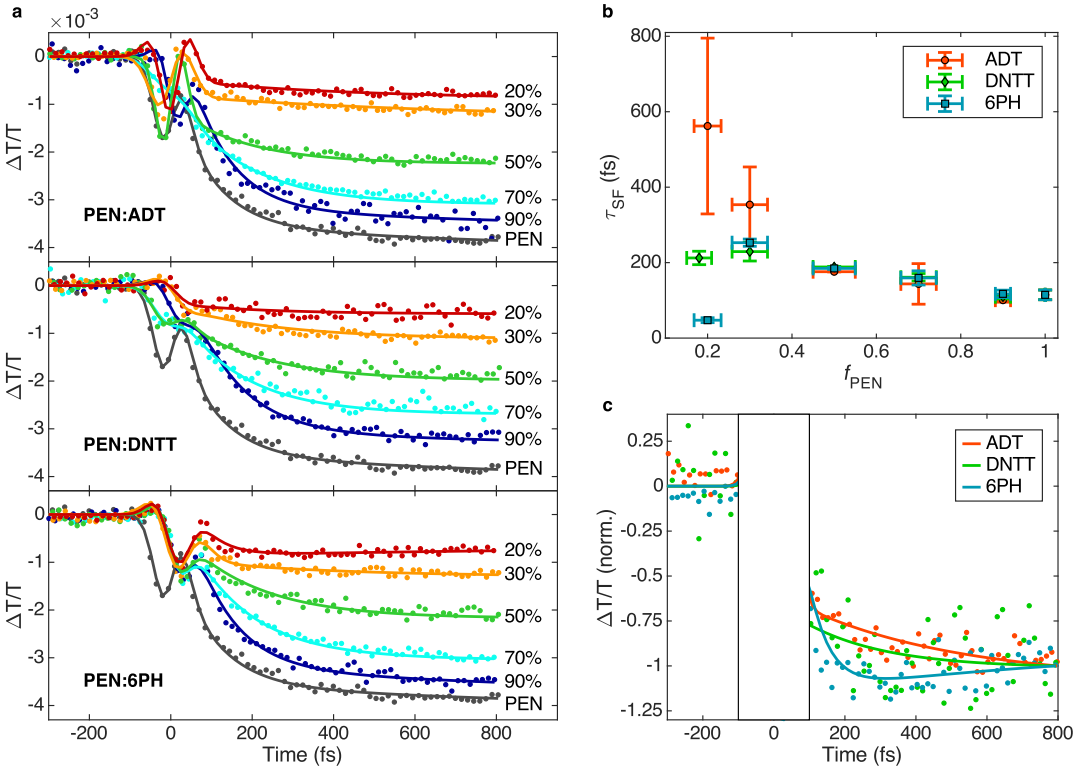

Figure 4. TA data analysis. (a) Time traces for all blends at a wavelength of 860 nm (1.44 eV), corresponding to the triplet ESA, along with the fit results from global analysis (solid lines). (b) Comparison of the SF time constant τ_{SF} from global analysis for different f_{PEN} and spacer molecules. (c) Time traces for the 20% blends at the position of the triplet ESA normalized to the fit value after 800 fs. Note that in the 20% blends, the coherent artifact from the temporal overlap of pump and probe pulse increases in weight compared to the actual signal and is therefore omitted for clarity.

assume the energy of ^{1}(TT) is the same for all blends in this work with $E(^1(TT)) = 2E(T_1) = 1.72$ eV,[24,40,48] independent of f_{PEN} and choice of spacer molecule (see Section S3.4 in the Supporting Information for details). As discussed below, this is also consistent with the theoretical model used for describing SF in the blends. Therefore, the change in $E(S_1)$ corresponds to an energetic shift of S_1 compared to ^{1}(TT) and its higher vibrational sublevels, including those involving one or two vibrational quanta, denoted $^1(TT)^{\star}$ and $^1(TT)^{\star\star}$, respectively. In neat PEN, S_1 has been proposed to be resonant with $^1(TT)^{\star}$,[22,24] and increasing the spacer fraction results in the break-up of this resonance by shifting S_1 to higher energy. This can be clearly seen in Figure 2c, where the energies of $^1(TT)^{\star}$ and $^1(TT)^{\star\star}$ are additionally shown as gray horizontal lines superimposed by a Gaussian energy distribution due to possible inhomogeneous broadening. However, since a recent theoretical study has found that inhomogeneous line broadening has only a negligible effect on SF,[54] it is not considered further in our study. For the vibrational spacing, we assumed an energy of 143 meV (1150 cm^{-1}) recently proposed as a crucial vibrational mode facilitating SF of PEN.[22,24] Note that only for 6PH, the difference in polarizability is large enough to bring S_1 into resonance with $^1(TT)^{\star\star}$ for small PEN fractions. This constitutes the first important result of our work, namely, our ability to vary the energetic difference between S_1 and ^{1}(TT) continuously within an energy range of $\Delta E \approx 150$ meV, corresponding to the difference between two vibrational energy levels of the above-mentioned relevant mode, by using different spacer molecules and mixing ratios. Accordingly, our approach allows us to elucidate the role of specific vibrational modes in mediating SF through vibronic coupling by measuring the evolution of the SF time constant, τ_{SF}, with femtosecond TA spectroscopy.

Figure 3a–d reports the TA spectra for neat PEN and the 20% PEN blends in the wavelength range between 550 (2.25 eV) and 950 nm (1.31 eV), covering the ground-state bleach (GSB), the stimulated emission (SE), and the triplet excited-state absorption (ESA) in PEN.[55] For these experiments, the pump wavelength is chosen at 620 nm (2.00 eV for blends with ADT) and 610 nm (2.03 eV for blends with DNTT and 6PH) in order to consistently excite the upper Davydov component of PEN while remaining below the band gap of the respective spacer molecules. The spacing to the vibronic progression of the SE at 725 nm (1.71 eV) is approximately 140 meV. The rise of the triplet ESA for wavelengths above 770 nm (below 1.6 eV) gives a direct measure of τ_{SF}.[19,40,55,56]

We focus our analysis on the blends with 20% PEN (Figure 3b–d) for which our steady-state optical characterization revealed the largest shift of $E(S_1)$ and for which therefore the most distinct differences in the SF kinetics can be expected. Compared to neat PEN, the position of the strongest TA feature is shifted to shorter wavelengths and matches the energy of the upper Davydov component. It is likely that SE from monomeric PEN, isolated in a matrix of spacer molecules, overlaps with the GSB here, indicating a more complex photophysical behavior. The smaller peak between 650 nm (1.9 eV) and 690 nm (1.8 eV) comprises a GSB of the lower Davydov component along with SE. We note that this feature is preserved on the picosecond timescale which can be rationalized by SE from long-lived monomeric PEN.[32,33,44] Furthermore, it might be possible that SE from ^{1}(TT), which has been demonstrated to contribute to the emission spectrum in PEN,[57] contributes to this feature. The

https://doi.org/10.1021/jacs.2c07237
J. Am. Chem. Soc. 2022, 144, 20610–20619

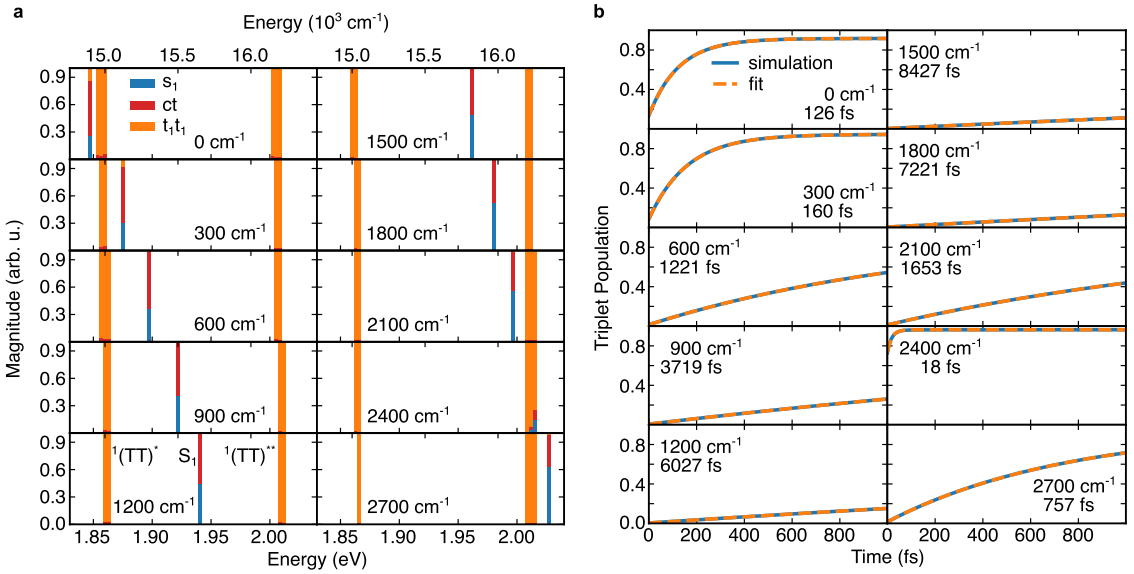

Figure 5. Simulation of SF in the blends. (a) Composition of adiabatic states with different ΔE_{ct} inset within each plot. All other parameters remain constant. Only states for which the transition from the ground state has finite (non-zero) oscillator strength are shown (see refs 23 and 24). For visual clarity, each line represents the average composition of states with energies that lie within the width of the bar (25 cm^{-1}). (b) Triplet population as a function of time for 2 × 2 crystals with different ΔE_{ct}. ΔE_{ct} for each simulation is shown in the figure inset, along with the SF time constant τ_{SF}.

observation of triplet ESA above 770 nm (below 1.6 eV) proves the existence of SF even at such low PEN fractions.

A comparison of the evolution of the TA signal in the spectral region of the triplet ESA is shown in Figure 3e. The first important observation is the ascending order of the absolute TA signal at early times (0−0.1 ps) with increasing optical band gap of the spacer molecule. This behavior is indicative of different triplet-pair state admixtures to the initially excited adiabatic S_1 state, consistent with the coherent nature[10,15,29,58,59] of the SF process in PEN[13,28,33] and the crystalline structure in our blends. Following the temporal evolution of the triplet ESA for the two extreme cases, 6PH and ADT, a continuous increase is observed for ADT even up to the longest time delays, while for 6PH, the build-up is already complete after approximately 200 fs. Last, the evolution of the triplet ESA in DNTT is intermediate to the blends with the other two spacer molecules.

To quantify τ_{SF} for all blends, we analyzed the TA data by global analysis using the software GloTarAn (see SI for details on the fitting procedure).[60] A comparison between measured data and fit results based on a sequential model for time traces at 860 nm (1.44 eV) representing the triplet ESA is shown in Figure 4a (see Figures S23 and S42 in the Supporting Information for details). We note that the decrease of the absolute TA intensity in the triplet ESA (Figure 4a) for decreasing PEN fraction is due to the reduced total number of PEN molecules. As SF in PEN is known to proceed with a time constant of approximately 100 fs,[55,61] focus is given to the early delay times.

The resulting τ_{SF} are shown in Figure 4b and give a similar trend for blends with excess of PEN ($f_{PEN} > 0.5$), independent of the spacer molecule. This changes dramatically toward lower PEN fraction. For the spacer molecule with largest polarizability, ADT, τ_{SF} continues to increase with decreasing f_{PEN}, while we observe a sudden drop in τ_{SF} for 6PH. This leads to a clear ordering in τ_{SF} for the different spacer molecules, especially for $f_{PEN} = 0.2$, which follows the trend in optical band gap and polarizability (Figure 1c). This can also be seen qualitatively by comparing the corresponding time traces of the triplet ESA, see Figure 4c. Despite the larger error bar for τ_{SF} at low f_{PEN} in blends with ADT, both the qualitative and quantitative analysis demonstrate the dependence of the SF kinetics on the energetic difference between S_1 and ^{1}(TT), controlled by the choice of spacer molecule and the mixing ratio.

To elucidate the role of energetic resonance in the observed evolution of τ_{SF}, we modeled the SF process based on a previously developed model[23,24] that treats both electronic and vibrational degrees of freedom on equal footing (see Methods and Supporting Information for details). The model considers three types of diabatic electronic states: singlet Frenkel excitons denoted by s_1, charge-transfer excitons denoted by ct, and correlated triplet-pair excitons denoted by t_1t_1, all of which play an important role in the SF process.[7−9,14,15,17−19] The model also treats a single vibrational mode at 1150 cm^{-1} quantum mechanically. This mode has been identified in the literature as an important mode for mediating singlet fission in pentacene.[24] While it is likely that other nearby vibrational modes could also play a role in the SF process and are likely necessary to quantitatively reproduce the experimental data, including these modes is beyond the scope of the current paper and our computational resources. We note, however, that recent advances using tensor network simulations[27,62] appear promising for overcoming the challenges associated with the simultaneous quantum treatment of several vibrational modes and think that this would be a worthwhile pursuit for future studies. Moreover, we assign the same vibrational energy to all diabatic electronic states (s_1, ct, and t_1) even though the vibrational energies for these states are expected to be slightly different due to the differences in their potential energy surfaces. However, we do not anticipate that this approximation will affect the results of our simulations in a significant way. In the following discussion, diabatic states are labeled with lowercase letters s_1, t_1t_1, and ct, while adiabatic states are labeled with uppercase letters S_1 and ^{1}(TT), following ref 23.

To investigate the effect of varying $E(S_1)$ on τ_{SF}, we systematically increase the energy of the diabatic ct states from the value in neat pentacene, $\Delta E_{ct} = 0$ to $\Delta E_{ct} = 2700$ cm^{-1} (see

https://doi.org/10.1021/jacs.2c07237
J. Am. Chem. Soc. 2022, 144, 20610−20619

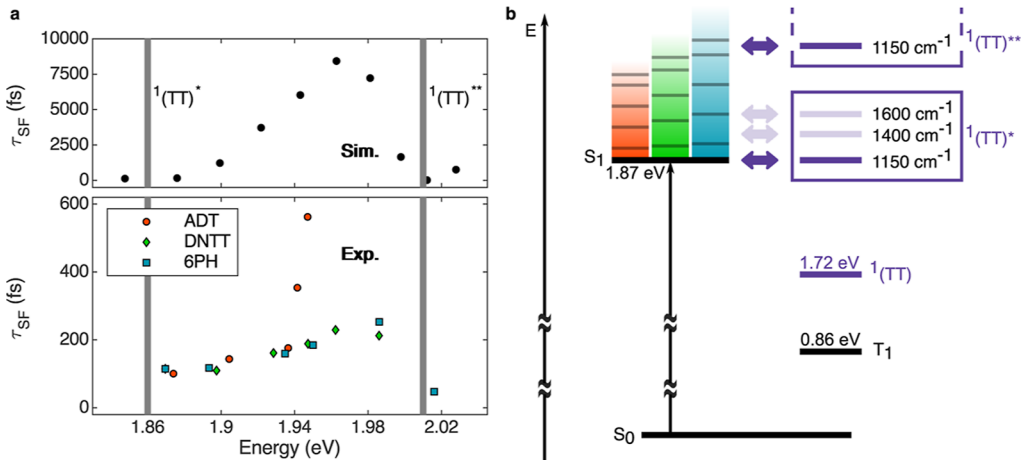

Figure 6. SF time constants and vibronic coupling scheme. (a) Comparison between the simulated SF time constants (top) and the experimentally determined SF time constants (bottom). The trend with respect to energy $E(S_1)$ is the same while they differ in the absolute values (see text for details). The positions of the first and second vibrational sublevel of ^{1}(TT) are shown as vertical gray bars, with an energy spacing of 1150 cm^{-1}. (b) Proposed scheme of the modification of vibronic coupling in the PEN blends. Energetic resonance between S_1 and the vibrational sublevels of ^{1}(TT) is achieved by increasing $E(S_1)$ through polarization effects induced by the presence of spacer molecules as indicated by the color gradient boxes. Changing the mixing ratio in the blends allows for minute control of the energetic position. Strong vibronic coupling occurs for S_1 being resonant with ^{1}(TT) dressed by one or two vibrational quanta with a vibrational frequency of 1150 cm^{-1}, while other vibrational modes play a minor role for efficient coupling between the relevant states in SF.

Figure 5). The justification for varying the energies of the diabatic ct states is that they are expected to be most sensitive to the environmental polarizability. The localized nature of the diabatic s_1 and t_1t_1 states implies that they are much less sensitive to changes in the environmental polarizability. Since the adiabatic states, S_1 and ^{1}(TT), are composed of the diabatic states, s_1, ct, and t_1t_1, it is the varying ct contribution which controls the sensitivity to the molecular environment, see Figure 5a and Table S1 in the Supporting Information. The above-mentioned values of the diabatic ct energy bring $E(S_1)$ from its value in neat PEN to just above $E(^1(TT)^{\star\star})$. Figure 5a shows the diabatic character of the adiabatic states with non-zero oscillator strength as ΔE_{ct} is varied. Within these plots, the adiabatic S_1, $^1(TT)^{\star}$, and $^1(TT)^{\star\star}$ states are readily identified. The $^1(TT)^{\star}$ and $^1(TT)^{\star\star}$ clusters are approximately separated by the vibrational energy, 1150 cm^{-1}, and have mainly diabatic t_1t_1 character. Importantly, the energies of the ^{1}(TT) states are robust against changes in ΔE_{ct} due to the relatively small ct character of these states (see Figure 5a). The simulations therefore support the assumption made earlier regarding the stability of ^{1}(TT) in the experimental systems with respect to changes in the environmental polarizability. The S_1 state always has mostly s_1 and ct character, but a noteworthy observation is the evolution of the admixture of t_1t_1 to the initially excited S_1 state with increasing ΔE_{ct}. When S_1 is near resonance with $^1(TT)^{\star}$ (see ΔE_{ct} = 0 and ΔE_{ct} = 300 cm^{-1}), a significant contribution from t_1t_1 is found. The contribution from t_1t_1 becomes negligible for increasing ΔE_{ct} but reappears once S_1 comes into resonance with $^1(TT)^{\star\star}$ (ΔE_{ct} = 2400 cm^{-1}). This is particularly important for our study as the initial t_1t_1 contribution is directly linked to the SF time constant.[16,33] The mixing between the diabatic s_1 and t_1t_1 is mediated by ct states,[14] as can be seen by the ct admixture to both S_1 and the vibrationally dressed ^{1}(TT) (see Figure 5b and Table S1 in the Supporting Information). We note that, consistent with recent literature reports, a small but non-vanishing ct contribution to the triplet-pair state is sufficient to facilitate ultrafast SF in PEN.[16,38,58] To extract τ_{SF}, the temporal evolution of the diabatic triplet population is fitted to an exponential function, see Figure 5b and the Supporting Information for details.

Figure 6 summarizes the SF time constants as a function of $E(S_1)$. In the simulation (upper panel in Figure 6a), τ_{SF} increases as $E(S_1)$ increases and S_1 moves out of resonance with $^1(TT)^{\star}$. A further increase in $E(S_1)$ leads to S_1 approaching $^1(TT)^{\star\star}$ and results in a reduction of τ_{SF}. If S_1 is resonant with $^1(TT)^{\star\star}$, τ_{sf} has a similar value as in neat PEN. Comparing the simulations with the experiment (lower panel in Figure 6a), we find that they qualitatively capture the experimentally observed behavior. In particular, the agreement in the energy at which τ_{SF} begins to decrease (around 1.96−1.98 eV) is the central result of our study since it demonstrates the sensitivity of τ_{SF} to vibrational modes near 1150 cm^{-1}. This result is summarized by the scheme shown in Figure 6b.

We note that the discrepancy between the experiment and simulation for intermediate values of $E(S_1)$ (see Figure 6a) likely has some origin in the model approximations. For example, the simulations only treat one vibrational mode at 1150 cm^{-1} (143 meV) quantum mechanically, but coupling to other vibrational modes, inter alia modes at 1400 cm^{-1} (174 meV) and 1600 cm^{-1} (198 meV)[7,23,24,63] may also lead to a reduction in τ_{SF} as S_1 passes through resonance with the corresponding vibrationally excited triplet-pair states. It is also possible that the low-frequency spectral density, which is taken to be of the Debye form, is not accurate.[24] Another discrepancy between the model and experiment is the presence of the spacer molecules. The current model mimics the effects of the spacer molecules by varying ΔE_{ct} for the individual PEN molecules, while in reality, the situation is more nuanced. In ref 32, the spacer molecules were accounted for in more detail by adjusting the PEN−PEN transfer integrals to account for packing variation within the crystalline lattice and a significantly increased τ_{SF} was predicted. Since the spacer molecules used in this study have been chosen to preserve the intermolecular packing as much as possible, we expect variations in the charge-transfer integrals to be minimal

https://doi.org/10.1021/jacs.2c07237
J. Am. Chem. Soc. 2022, 144, 20610−20619

and only have minor effects on the qualitative aspects of the model predictions. We have therefore omitted consideration of changes in the charge-transfer integrals in this study. In ref 33, focus was given to the replacement of nearest neighbors, and the robustness of the SF rate observed in ref 32 was explained by the coherence of the process. A realistic simulation of the full system combining both approaches exceeds the scope of this work. However, an insight into the multiple contributions to variations in the SF rate for such blends can be gained from the experiment by comparing the series with three different spacer molecules. These contributions include the above-mentioned replacement of nearest neighbors and changes in the unit cell with corresponding changes in intermolecular distances[14] and/or molecular orientation.[16,64] Both have an impact on intermolecular interactions and charge-transfer state admixture to S_1,[7−9,14,15,17−19,65] which mediates the SF process in PEN.[14,18,21] Additionally, the entropic gain during SF is reduced in blends due to a reduction of possible microstates by replacing the nearest neighbors or confining the singlet exciton.[66]

We start by excluding the impact of the expansion of the unit cell, focusing on the in-plane parameters known to be central for the photophysics in PEN.[24,32] The largest change in τ_{SF} is observed for ADT as a spacer molecule for which almost no change in in-plane unit cell parameters is observed (see Figure S4 in the Supporting Information), while τ_{SF} shows the smallest increase for 6PH blends despite the largest geometrical changes. We note that the decreasing crystallite size and corresponding coherence length of the singlet exciton for larger ADT concentrations might be a possible explanation for the strong increase in τ_{SF} for low PEN fraction with ADT as the spacer molecule.[67] This increased structural disorder reduces the coherence length of the singlet exciton, the number density of the final ^{1}(TT) states, and, thus, also the SF rate.[54,67−69] In contrast, an effect of the crystallite size can be excluded for the other two systems (see Figure S5 in the Supporting Information).[11] Last, we note that an exciton migration determined SF process would lead to monotonically increasing SF time constants for decreasing PEN fraction and should result in the smallest SF rates for blends of PEN with 6PH due to the largest increase in in-plane lattice parameters and is thus not supported by our data. Next, we turn to the impact of intermolecular interactions and charge-transfer admixture to S_1 on τ_{SF}. The DS can serve as a measure for this parameter[14,34] but shows for all blends the same trend (see Figure S8 in the Supporting Information), supporting the idea that already a small charge-transfer admixture to S_1 is sufficient to facilitate fast SF.[16,58] This is also supported by the simulation results presented in Figure 5 which show that the ct admixture to S_1 decreases significantly as ΔE_{ct} increases. Despite the decrease in the ct admixture, τ_{SF} still decreases dramatically when S_1 is nearly resonant with ^{1}(TT)**. Last, an effect from entropic gain as a driving force for SF[70] can be ruled out in our blends. The number of microstates for ^{1}(TT) continuously decreases with increasing spacer concentration, leading to a reduction in entropy and should result in a slowdown in SF, which is incompatible with the acceleration of τ_{SF} for low PEN concentration with 6PH as the spacer molecule. This leaves the impact of the vibronic coupling as the main parameter determining τ_{SF} in these blends and demonstrates the potential of our approach to control the coupling efficiency by continuously scanning S_1 through energetic resonance with ^{1}(TT) and its vibrational sublevels.

Our interpretation of the decrease of the SF time constant for the blend with 20% PEN and 80% 6PH being due to vibronic coupling is further supported by an in-depth analysis of our TA data in the spectral region of the triplet ESA band between 780 and 950 nm (see Section S4.3 in the Supporting Information for details). The dip visible in the time traces around 300 fs (see Figures 4 and S39−S42 in the Supporting Information) is reproduced by a sequential model, in which the electronic ^{1}(TT)** state containing two vibrational quanta serves as an intermediate state from which the vibrationally relaxed electronic ^{1}(TT) state is populated via vibrational relaxation.[71,72] The time constant determined using this sequential model is approximately 800 fs and therefore in a similar range as vibrational relaxation in PEN[73] and comparable systems,[71,72] supporting our interpretation that the coupling to a vibrationally excited state causes the observed decrease of the SF time constant.

CONCLUSIONS

In summary, by using blends to engineer the polarizability of the molecular environment, we control the energetic difference between S_1 and vibrational sublevels of ^{1}(TT) in PEN. Changing the spacer molecule and mixing ratio in PEN blends, we were able to scan over a variety of vibrational modes and probe the concomitant evolution of τ_{SF} with TA spectroscopy. After an initial increase in τ_{SF} due to unfavorable energetic offset between S_1 and ^{1}(TT), we observed a clear difference in the trend between the series with the three spacer molecules toward reduced f_{PEN}. Only for the blends with the spacer molecule of lowest polarizability, an acceleration of the SF process was found; this result was interpreted in terms of S_1 coming into resonance with the doubly vibrationally excited triplet-pair state, ^{1}(TT)**. Based on a comparison with simulation, we identified vibrational modes near 1150 cm^{-1} as the origin for this acceleration. Thus, our study emphasizes the important role that vibronic coupling plays in facilitating ultrafast SF in PEN. By scanning S_1 relative to ^{1}(TT), we gain insight into microscopic details which go beyond the existing approaches. As a general perspective, such blends have the potential for the study of the impact of energetic resonance between electronically and vibronically excited states in a variety of complex photophysical processes as they enable a continuous and fine tuning of excited-state energetics.

EXPERIMENTAL SECTION

The mixed films of PEN (Sigma Aldrich, 99.99%, triple sublimed), ADT (Sigma-Aldrich, 97%), DNTT (Sigma-Aldrich, 99%), and 6PH (Lambson Japan Co. Ltd. 99%) were grown by organic molecular beam deposition on silicon with a native oxide layer (Microchemicals) and on borofloat glass substrates (Menzel coverslip) at a base pressure of 1×10^{-8} mbar. The total growth rate was 0.6 nm/min, with the rates of the two materials monitored separately by two quartz crystal microbalances, calibrated using X-ray reflectivity. The final film thickness was 80 nm.

UV−vis transmission spectra were recorded using a PerkinElmer Lambda 950 spectrophotometer.

Ultrafast pump probe experiments were performed using a Ti/Sapphire chirped pulse amplified source (Coherent Libra), with 4 mJ output energy, 1 kHz repetition rate, 800 nm central wavelength, and 100 fs pulse duration. Excitation pulses at 620 nm (for samples with ADT) and 610 nm (for samples with DNTT and 6PH to consistently excite above the energy of the upper Davydov component) with 70 fs duration were generated by non-collinear optical parametric amplification in a β-barium borate crystal. Pump pulses were focused

https://doi.org/10.1021/jacs.2c07237
J. Am. Chem. Soc. 2022, 144, 20610−20619

to an approximately 400 μm diameter spot. Probing was achieved in the visible and near-infrared region (530 to 1000 nm) by using a white light continuum generated in a 5 mm YAG plate. Transient transmission spectra were collected by using a fast optical multichannel analyzer. The measured quantities are the transmission with (T_p) and without (T) prior excitation by the pump pulse from which the differential transmission, $\Delta T/T$, is calculated as $\Delta T/T = (T_p - T)/T$. For excitation, a fluence of 32 μJ/cm^2 was used for all samples. Measurements were performed at room temperature and under vacuum or in protective atmosphere to avoid sample degradation. For the global analysis of the obtained TA data, the open-source software GloTarAn was used.[60]

SF dynamics are calculated using Redfield theory according to the model and methods described in refs 23 and 24. As in ref 24, the dynamics are simulated for 2 × 2 neat pentacene crystals initialized in the adiabatic S_1 state and using parameters that reproduce the experimental S_1 and ^{1}(TT) energies. Holstein vibronic coupling to the 1150 cm^{-1} intramolecular vibrational mode is included, while all other vibrational modes, including the intermolecular modes that contribute to non-local Peierls interactions, are included in the Debye spectral density used in the Redfield calculations. We note that Peierls-type vibronic coupling was shown in ref 24 to only have a modest effect on SF. To simulate the effect of the changing environmental polarizability due to the replacement of PEN molecules with spacer molecules, the energy of the diabatic ct states is adjusted. All other parameters are the same as in ref 24 except the cut-off used to truncate the Redfield calculations, which is increased from 15,500 to 16,450 cm^{-1} to ensure that all relevant adiabatic states are included in the calculation for every ΔE_{ct} energy considered.

■ ASSOCIATED CONTENT

Supporting Information

The Supporting Information is available free of charge at https://pubs.acs.org/doi/10.1021/jacs.2c07237.

Details on experimental methods; details on structural analysis including X-ray reflectivity and grazing incidence wide-angle X-ray scattering data, probability for the number of nearest neighbors in the blends, UV−vis absorption spectra and analysis, temperature-dependent photoluminescence spectra, transient absorption data and analysis; and details on the simulations (PDF)

■ AUTHOR INFORMATION

Corresponding Authors

Nicholas J. Hestand − *Department of Natural and Applied Sciences, Evangel University, Springfield, Missouri 65802, United States;* orcid.org/0000-0001-7522-2466; Email: hestandn@evangel.edu

Giulio Cerullo − *Dipartimento di Fisica, Politecnico di Milano, Milan 20133, Italy;* orcid.org/0000-0002-9534-2702; Email: giulio.cerullo@polimi.it

Katharina Broch − *Institute for Applied Physics, University of Tuebingen, Tuebingen 72076, Germany;* orcid.org/0000-0002-9354-292X; Email: brochkatharina@gmail.com

Authors

Frederik Unger − *Institute for Applied Physics, University of Tuebingen, Tuebingen 72076, Germany;* orcid.org/0000-0002-7127-3829

Luca Moretti − *Dipartimento di Fisica, Politecnico di Milano, Milan 20133, Italy;* orcid.org/0000-0001-8092-0752

Julian Hausch − *Institute for Applied Physics, University of Tuebingen, Tuebingen 72076, Germany*

Jona Bredehoeft − *Institute for Applied Physics, University of Tuebingen, Tuebingen 72076, Germany*

Clemens Zeiser − *Institute for Applied Physics, University of Tuebingen, Tuebingen 72076, Germany;* orcid.org/0000-0003-3613-2243

Sara Haug − *Institute for Applied Physics, University of Tuebingen, Tuebingen 72076, Germany*

Roel Tempelaar − *Department of Chemistry, Northwestern University, Evanston, Illinois 60208, United States;* orcid.org/0000-0003-0786-7304

Complete contact information is available at: https://pubs.acs.org/10.1021/jacs.2c07237

Author Contributions

$^{\perp}$L.M. and J.H. contributed equally.

Notes

The authors declare no competing financial interest.

■ ACKNOWLEDGMENTS

The authors thank Prof. Frank Schreiber (University of Tübingen) for access to equipment, Dr. Margherita Maiuri (Politecnico di Milano) for scientific support, and Dr. Benjamin Unger (University of Stuttgart) for fruitful discussion. The research leading to these results has received funding from LASERLAB-EUROPE (grant agreement no. 871124, project: CUSBO002712, European Union's Horizon 2020 research and innovation programme). F.U. and K.B. acknowledge funding from the German Research Foundation (BR 4869/4−1).

■ REFERENCES

(1) Hanna, M. C.; Nozik, A. J. Solar conversion efficiency of photovoltaic and photoelectrolysis cells with carrier multiplication absorbers. *J. Appl. Phys.* **2006**, *100*, 074510.

(2) Smith, M. B.; Michl, J. Singlet Fission. *Chem. Rev.* **2010**, *110*, 6891−6936.

(3) Miyata, K.; Conrad-Burton, F. S.; Geyer, F. L.; Zhu, X.-Y. Triplet Pair States in Singlet Fission. *Chem. Rev.* **2019**, *119*, 4261−4292.

(4) Smith, M. B.; Michl, J. Recent Advances in Singlet Fission. *Annu. Rev. Phys. Chem.* **2013**, *64*, 361−386.

(5) Johnson, R. C.; Merrifield, R. E. Effects of Magnetic Fields on the Mutual Annihilation of Triplet Excitons in Anthracene Crystals. *Phys. Rev. B* **1970**, *1*, 896−902.

(6) Müller, U.; Roos, L.; Frank, M.; Deutsch, M.; Hammer, S.; Krumrein, M.; Friedrich, A.; Marder, T. B.; Engels, B.; Krueger, A.; Pflaum, J. Role of Intermolecular Interactions in the Excited-State Photophysics of Tetracene and 2,2′-Ditetracene. *J. Phys. Chem. C* **2020**, *124*, 19435−19446.

(7) Hart, S. M.; Silva, W. R.; Frontiera, R. R. Femtosecond stimulated Raman evidence for charge-transfer character in pentacene singlet fission. *Chem. Sci.* **2018**, *9*, 1242−1250.

(8) Chen, M.; Bae, Y. J.; Mauck, C. M.; Mandal, A.; Young, R. M.; Wasielewski, M. R. Singlet Fission in Covalent Terrylenediimide Dimers: Probing the Nature of the Multiexciton State Using Femtosecond Mid-Infrared Spectroscopy. *J. Am. Chem. Soc.* **2018**, *140*, 9184−9192.

(9) Mandal, A.; Chen, M.; Foszcz, E. D.; Schultz, J. D.; Kearns, N. M.; Young, R. M.; Zanni, M. T.; Wasielewski, M. R. Two-Dimensional Electronic Spectroscopy Reveals Excitation Energy-Dependent State Mixing during Singlet Fission in a Terrylenediimide Dimer. *J. Am. Chem. Soc.* **2018**, *140*, 17907−17914.

(10) Stern, H. L.; Cheminal, A.; Yost, S. R.; Broch, K.; Bayliss, S. L.; Chen, K.; Tabachnyk, M.; Thorley, K.; Greenham, N.; Hodgkiss, J. M.; Anthony, J.; Head-Gordon, M.; Musser, A. J.; Rao, A.; Friend, R. H. Vibronically coherent ultrafast triplet-pair formation and subsequent thermally activated dissociation control efficient endothermic singlet fission. *Nat. Chem.* **2017**, *9*, 1205−1212.

(11) Arias, D. H.; Ryerson, J. L.; Cook, J. D.; Damrauer, N. H.; Johnson, J. C. Polymorphism influences singlet fission rates in tetracene thin films. *Chem. Sci.* **2016**, *7*, 1185−1191.
(12) Piland, G. B.; Bardeen, C. J. How Morphology Affects Singlet Fission in Crystalline Tetracene. *J. Phys. Chem. Lett.* **2015**, *6*, 1841−1846.
(13) Seiler, H.; Krynski, M.; Zahn, D.; Hammer, S.; Windsor, Y. W.; Vasileiadis, T.; Pflaum, J.; Ernstorfer, R.; Rossi, M.; Schwoerer, H. Nuclear dynamics of singlet exciton fission in pentacene single crystals. *Sci. Adv.* **2021**, *7*, No. eabg0869.
(14) Beljonne, D.; Yamagata, H.; Brédas, J. L.; Spano, F. C.; Olivier, Y. Charge-Transfer Excitations Steer the Davydov Splitting and Mediate Singlet Exciton Fission in Pentacene. *Phys. Rev. Lett.* **2013**, *110*, 226402.
(15) Morrison, A. F.; Herbert, J. M. Evidence for Singlet Fission Driven by Vibronic Coherence in Crystalline Tetracene. *J. Phys. Chem. Lett.* **2017**, *8*, 1442−1448.
(16) Wang, L.; Olivier, Y.; Prezhdo, O. V.; Beljonne, D. Maximizing Singlet Fission by Intermolecular Packing. *J. Phys. Chem. Lett.* **2014**, *5*, 3345−3353.
(17) Renaud, N.; Grozema, F. C. Intermolecular Vibrational Modes Speed Up Singlet Fission in Perylenediimide Crystals. *J. Phys. Chem. Lett.* **2015**, *6*, 360−365.
(18) Monahan, N.; Zhu, X.-Y. Charge Transfer-Mediated Singlet Fission. *Annu. Rev. Phys. Chem.* **2015**, *66*, 601−618.
(19) Pensack, R. D.; Ostroumov, E. E.; Tilley, A. J.; Mazza, S.; Grieco, C.; Thorley, K. J.; Asbury, J. B.; Seferos, D. S.; Anthony, J. E.; Scholes, G. D. Observation of Two Triplet-Pair Intermediates in Singlet Exciton Fission. *J. Phys. Chem. Lett.* **2016**, *7*, 2370−2375.
(20) Alvertis, A. M.; Lukman, S.; Hele, T. J. H.; Fuemmeler, E. G.; Feng, J.; Wu, J.; Greenham, N. C.; Chin, A. W.; Musser, A. J. Switching between Coherent and Incoherent Singlet Fission via Solvent-Induced Symmetry Breaking. *J. Am. Chem. Soc.* **2019**, *141*, 17558−17570.
(21) Berkelbach, T. C.; Hybertsen, M. S.; Reichman, D. R. Microscopic theory of singlet exciton fission. II. Application to pentacene dimers and the role of superexchange. *J. Chem. Phys.* **2013**, *138*, 114103.
(22) Bakulin, A. A.; Morgan, S. E.; Kehoe, T. B.; Wilson, M. W. B.; Chin, A. W.; Zigmantas, D.; Egorova, D.; Rao, A. Real-time observation of multiexcitonic states in ultrafast singlet fission using coherent 2D electronic spectroscopy. *Nat. Chem.* **2016**, *8*, 16−23.
(23) Tempelaar, R.; Reichman, D. R. Vibronic exciton theory of singlet fission. I. Linear absorption and the anatomy of the correlated triplet pair state. *J. Chem. Phys.* **2017**, *146*, 174703.
(24) Tempelaar, R.; Reichman, D. R. Vibronic exciton theory of singlet fission. III. How vibronic coupling and thermodynamics promote rapid triplet generation in pentacene crystals. *J. Chem. Phys.* **2018**, *148*, 244701.
(25) Busby, E.; Berkelbach, T. C.; Kumar, B.; Chernikov, A.; Zhong, Y.; Hlaing, H.; Zhu, X.-Y.; Heinz, T. F.; Hybertsen, M. S.; Sfeir, M. Y.; Reichman, D. R.; Nuckolls, C.; Yaffe, O. Multiphonon Relaxation Slows Singlet Fission in Crystalline Hexacene. *J. Am. Chem. Soc.* **2014**, *136*, 10654−10660.
(26) Musser, A. J.; Liebel, M.; Schnedermann, C.; Wende, T.; Kehoe, T. B.; Rao, A.; Kukura, P. Evidence for conical intersection dynamics mediating ultrafast singlet exciton fission. *Nat. Phys.* **2015**, *11*, 352−357.
(27) Schnedermann, C.; Alvertis, A. M.; Wende, T.; Lukman, S.; Feng, J.; Schröder, F. A. Y. N.; Turban, D. H. P.; Wu, J.; Hine, N. D. M.; Greenham, N. C.; Chin, A. W.; Rao, A.; Kukura, P.; Musser, A. J. A molecular movie of ultrafast singlet fission. *Nat. Commun.* **2019**, *10*, 4207.
(28) Duan, H.-G.; Jha, A.; Li, X.; Tiwari, V.; Ye, H.; Nayak, P. K.; Zhu, X.-L.; Li, Z.; Martinez, T. J.; Thorwart, M.; Miller, R. J. D. Intermolecular vibrations mediate ultrafast singlet fission. *Sci. Adv.* **2020**, *6*, No. eabb0052.
(29) Monahan, N. R.; Sun, D.; Tamura, H.; Williams, K. W.; Xu, B.; Zhong, Y.; Kumar, B.; Nuckolls, C.; Harutyunyan, A. R.; Chen, G.; Dai, H.-L.; Beljonne, D.; Rao, Y.; Zhu, X.-Y. Dynamics of the triplet-pair state reveals the likely coexistence of coherent and incoherent singlet fission in crystalline hexacene. *Nat. Chem.* **2017**, *9*, 341−346.
(30) Folie, B. D.; Haber, J. B.; Refaely-Abramson, S.; Neaton, J. B.; Ginsberg, N. S. Long-Lived Correlated Triplet Pairs in a π-Stacked Crystalline Pentacene Derivative. *J. Am. Chem. Soc.* **2018**, *140*, 2326−2335.
(31) Chen, Y.; Shen, L.; Li, X. Effects of Heteroatoms of Tetracene and Pentacene Derivatives on Their Stability and Singlet Fission. *J. Phys. Chem. A* **2014**, *118*, 5700−5708.
(32) Broch, K.; Dieterle, J.; Branchi, F.; Hestand, N. J.; Olivier, Y.; Tamura, H.; Cruz, C.; Nichols, V. M.; Hinderhofer, A.; Beljonne, D.; Spano, F. C.; Cerullo, G.; Bardeen, C. J.; Schreiber, F. Robust singlet fission in pentacene thin films with tuned charge transfer interactions. *Nat. Commun.* **2018**, *9*, 954.
(33) Zeiser, C.; Cruz, C.; Reichman, D. R.; Seitz, M.; Hagenlocher, J.; Chronister, E. L.; Bardeen, C. J.; Tempelaar, R.; Broch, K. Vacancy control in acene blends links exothermic singlet fission to coherence. *Nat. Commun.* **2021**, *12*, 5149.
(34) Yamagata, H.; Norton, J.; Hontz, E.; Olivier, Y.; Beljonne, D.; Brédas, J. L.; Silbey, R. J.; Spano, F. C. The nature of singlet excitons in oligoacene molecular crystals. *J. Chem. Phys.* **2011**, *134*, 204703.
(35) Cudazzo, P.; Gatti, M.; Rubio, A. Excitons in molecular crystals from first-principles many-body perturbation theory: Picene versus pentacene. *Phys. Rev. B* **2012**, *86*, 195307.
(36) Tiago, M. L.; Northrup, J. E.; Louie, S. G. Ab initio calculation of the electronic and optical properties of solid pentacene. *Phys. Rev. B* **2003**, *67*, 115212.
(37) Sharifzadeh, S.; Darancet, P.; Kronik, L.; Neaton, J. B. Low-Energy Charge-Transfer Excitons in Organic Solids from First-Principles: The Case of Pentacene. *J. Phys. Chem. Lett.* **2013**, *4*, 2197−2201.
(38) Zeng, T.; Hoffmann, R.; Ananth, N. The low-lying electronic states of pentacene and their roles in singlet fission. *J. Am. Chem. Soc.* **2014**, *136*, 5755−5764.
(39) Zimmerman, P. M.; Zhang, Z.; Musgrave, C. B. Singlet fission in pentacene through multi-exciton quantum states. *Nat. Chem.* **2010**, *2*, 648−652.
(40) Wilson, M. W. B.; Rao, A.; Ehrler, B.; Friend, R. H. Singlet Exciton Fission in Polycrystalline Pentacene: From Photophysics toward Devices. *Acc. Chem. Res.* **2013**, *46*, 1330−1338.
(41) Köhler, A.; Bässler, H. *Electronic Processes in Organic Semiconductors: An Introduction*; John Wiley & Sons: Weinheim, 2015.
(42) Kitaigorodsky, A. I. *Mixed Crystals*; Springer-Verlag: Berlin, Heidelberg, 1984.
(43) Vegard, L. Die Konstitution der Mischkristalle und die Raumfüllung der Atome. *Zeitschrift für Physik* **1921**, *5*, 17−26.
(44) Lubert-Perquel, D.; Salvadori, E.; Dyson, M.; Stavrinou, P. N.; Montis, R.; Nagashima, H.; Kobori, Y.; Heutz, S.; Kay, C. W. M. Identifying triplet pathways in dilute pentacene films. *Nat. Commun.* **2018**, *9*, 4222.
(45) Toccoli, T.; Bettotti, P.; Cassinese, A.; Gottardi, S.; Kubozono, Y.; Loi, M. A.; Manca, M.; Verucchi, R. Photophysics of Pentacene-Doped Picene Thin Films. *J. Phys. Chem. C* **2018**, *122*, 16879−16886.
(46) Pensack, R. D.; Tilley, A. J.; Parkin, S. R.; Lee, T. S.; Payne, M. M.; Gao, D.; Jahnke, A. A.; Oblinsky, D. G.; Li, P.-F.; Anthony, J. E.; Seferos, D. S.; Scholes, G. D. Exciton Delocalization Drives Rapid Singlet Fission in Nanoparticles of Acene Derivatives. *J. Am. Chem. Soc.* **2015**, *137*, 6790−6803.
(47) Hirayama, S.; Lampert, R. A.; Phillips, D. Photophysics of meso-substituted anthracenes. Part 1.—Solutions and isolated vapours. *J. Chem. Soc., Faraday Trans.* **1985**, *81*, 371−382.
(48) Burgos, J.; Pope, M.; Swenberg, C. E.; Alfano, R. R. Heterofission in pentacene-doped tetracene single crystals. *Phys. Status Solidi B* **1977**, *83*, 249−256.
(49) Hellner, C.; Lindqvist, L.; Roberge, P. C. Absorption spectrum and decay kinetics of triplet pentacene in solution, studied by flash photolysis. *J. Chem. Soc., Faraday Trans.* **1972**, *68*, 1928.
(50) Ehrler, B.; Walker, B. J.; Böhm, M. L.; Wilson, M. W.; Vaynzof, Y.; Friend, R. H.; Greenham, N. C. In situ measurement of exciton

energy in hybrid singlet-fission solar cells. *Nat. Commun.* **2012**, *3*. DOI: 10.1038/ncomms2012
(51) Teichen, P. E.; Eaves, J. D. Collective aspects of singlet fission in molecular crystals. *J. Chem. Phys.* **2015**, *143*, 044118.
(52) Yong, C. K.; et al. The entangled triplet pair state in acene and heteroacene materials. *Nat. Commun.* **2017**, *8*, 15953.
(53) Bayliss, S. L.; Chepelianskii, A. D.; Sepe, A.; Walker, B. J.; Ehrler, B.; Bruzek, M. J.; Anthony, J. E.; Greenham, N. C. Geminate and Nongeminate Recombination of Triplet Excitons Formed by Singlet Fission. *Phys. Rev. Lett.* **2014**, *112*, 238701.
(54) Climent, C.; Casanova, D.; Feist, J.; Garcia-Vidal, F. J. Not dark yet for strong light-matter coupling to accelerate singlet fission dynamics. *Cell Rep. Phys. Sci.* **2022**, *3*, 100841.
(55) Wilson, M. W. B.; Rao, A.; Clark, J.; Kumar, R. S. S.; Brida, D.; Cerullo, G.; Friend, R. H. Ultrafast Dynamics of Exciton Fission in Polycrystalline Pentacene. *J. Am. Chem. Soc.* **2011**, *133*, 11830−11833.
(56) Khan, S.; Mazumdar, S. Theory of Transient Excited State Absorptions in Pentacene and Derivatives: Triplet−Triplet Biexciton versus Free Triplets. *J. Phys. Chem. Lett.* **2017**, *8*, 5943−5948.
(57) Bossanyi, D. G.; Matthiesen, M.; Wang, S.; Smith, J. A.; Kilbride, R. C.; Shipp, J. D.; Chekulaev, D.; Holland, E.; Anthony, J. E.; Zaumseil, J.; Musser, A. J.; Clark, J. Emissive spin-0 triplet-pairs are a direct product of triplet−triplet annihilation in pentacene single crystals and anthradithiophene films. *Nat. Chem.* **2021**, *13*, 163−171.
(58) Greyson, E. C.; Vura-Weis, J.; Michl, J.; Ratner, M. A. Maximizing Singlet Fission in Organic Dimers: Theoretical Investigation of Triplet Yield in the Regime of Localized Excitation and Fast Coherent Electron Transfer. *J. Phys. Chem. B* **2010**, *114*, 14168−14177.
(59) Schultz, J. D.; Shin, J. Y.; Chen, M.; O'Connor, J. P.; Young, R. M.; Ratner, M. A.; Wasielewski, M. R. Influence of Vibronic Coupling on Ultrafast Singlet Fission in a Linear Terrylenediimide Dimer. *J. Am. Chem. Soc.* **2021**, *143*, 2049−2058.
(60) Snellenburg, J. J.; Laptenok, S. P.; Seger, R.; Mullen, K. M.; van Stokkum; Glotaran, I. H. M. A Java-Based Graphical User Interface for the R Package TIMP. *J. Stat. Softw.* **2012**, *49*, 1−22.
(61) Jundt, C.; Klein, G.; Sipp, B.; Le Moigne, J. L.; Joucla, M.; Villaeys, A. Exciton dynamics in pentacene thin films studied by pump-probe spectroscopy. *Chem. Phys. Lett.* **1995**, *241*, 84−88.
(62) Schröder, F. A.; Turban, D. H.; Musser, A. J.; Hine, N. D.; Chin, A. W. Tensor network simulation of multi-environmental open quantum dynamics via machine learning and entanglement renormalisation. *Nat. Commun.* **2019**, *10*, 1−10.
(63) Hestand, N. J.; Yamagata, H.; Xu, B.; Sun, D.; Zhong, Y.; Harutyunyan, A. R.; Chen, G.; Dai, H.-L.; Rao, Y.; Spano, F. C. Polarized Absorption in Crystalline Pentacene: Theory vs Experiment. *J. Phys. Chem. C* **2015**, *119*, 22137−22147.
(64) Buchanan, E. A.; Michl, J. Packing Guidelines for Optimizing Singlet Fission Matrix Elements in Noncovalent Dimers. *J. Am. Chem. Soc.* **2017**, *139*, 15572−15575.
(65) Alam, B.; Morrison, A. F.; Herbert, J. M. Charge Separation and Charge Transfer in the Low-Lying Excited States of Pentacene. *J. Phys. Chem. C* **2020**, *124*, 24653−24666.
(66) Kolomeisky, A. B.; Feng, X.; Krylov, A. I. A Simple Kinetic Model for Singlet Fission: A Role of Electronic and Entropic Contributions to Macroscopic Rates. *J. Phys. Chem. C* **2014**, *118*, 5188−5195.
(67) Gish, M. K.; Thorley, K. J.; Parkin, S. R.; Anthony, J. E.; Johnson, J. C. Hydrogen Bonding Optimizes Singlet Fission in Carboxylic Acid Functionalized Anthradithiophene Films. *ChemPhotoChem* **2020**, *5*, 68−78.
(68) Pensack, R. D.; Grieco, C.; Purdum, G. E.; Mazza, S. M.; Tilley, A. J.; Ostroumov, E. E.; Seferos, D. S.; Loo, Y.-L.; Asbury, J. B.; Anthony, J. E.; et al. Solution-processable, crystalline material for quantitative singlet fission. *Mater. Horiz.* **2017**, *4*, 915−923.
(69) Grieco, C.; Doucette, G. S.; Pensack, R. D.; Payne, M. M.; Rimshaw, A.; Scholes, G. D.; Anthony, J. E.; Asbury, J. B. Dynamic exchange during triplet transport in nanocrystalline TIPS-pentacene films. *J. Am. Chem. Soc.* **2016**, *138*, 16069−16080.
(70) Chan, W.-L.; Ligges, M.; Zhu, X.-Y. The energy barrier in singlet fission can be overcome through coherent coupling and entropic gain. *Nat. Chem.* **2012**, *4*, 840−845.
(71) Cerullo, G.; Lanzani, G.; Zavelani-Rossi, M.; De Silvestri, S. D. Early events of energy relaxation in all-trans-β-carotene following sub-10 fs optical-pulse excitation. *Phys. Rev. B* **2001**, *63*, 241104.
(72) McCamant, D. W.; Kukura, P.; Mathies, R. A. Femtosecond Time-Resolved Stimulated Raman Spectroscopy: Application to the Ultrafast Internal Conversion in β-Carotene. *J. Phys. Chem. A* **2003**, *107*, 8208−8214.
(73) Hesselink, W. H.; Wiersma, D. A. Vibronic relaxation in molecular mixed crystals: Pentacene in naphthalene and *p*-terphenyl. *J. Chem. Phys.* **1981**, *74*, 886−889.

Recommended by ACS

Distinguishing between Triplet-Pair State and Excimer Emission in Singlet Fission Chromophores Using Mixed Thin Films
Julian Hausch, Katharina Broch, *et al.*
APRIL 08, 2022
THE JOURNAL OF PHYSICAL CHEMISTRY C
READ

Effects of the Separation Distance between Two Triplet States Produced from Intramolecular Singlet Fission on the Two-Electron-Transfer Process
Heyuan Liu, Xiyou Li, *et al.*
AUGUST 05, 2022
JOURNAL OF THE AMERICAN CHEMICAL SOCIETY
READ

Mechanism of Ultrafast Triplet Exciton Formation in Single Cocrystals of π-Stacked Electron Donors and Acceptors
Malik L. Williams, Michael R. Wasielewski, *et al.*
SEPTEMBER 30, 2022
JOURNAL OF THE AMERICAN CHEMICAL SOCIETY
READ

Using Molecular Design to Enhance the Coherence Time of Quintet Multiexcitons Generated by Singlet Fission in Single Crystals
Robert M. Jacobberger, Michael R. Wasielewski, *et al.*
JANUARY 31, 2022
JOURNAL OF THE AMERICAN CHEMICAL SOCIETY
READ

Get More Suggestions >